Nuclear Instruments and Methods in Physics Research A 1064 (2024) 169450

Contents lists available at ScienceDirect

Nuclear Inst. and Methods in Physics Research, A

journal homepage: www.elsevier.com/locate/nima

The importance of the adiabatic condition on polarized neutron imaging

U.K. Oji [a,b,*], A. Backs [c], W. Kockelmann [d], I. Manke [b], A. Hilger [b], N. Kardjilov [b], R. Cubitt [a]

[a] Institut Laue-Langevin, Large Scale Structures Group, 71 Avenue des Martyrs CS 20156, 38042, Grenoble Cedex 9, France
[b] Helmholtz Centre Berlin for Materials and Energy, D-14109, Berlin, Germany
[c] European Spallation Source ERIC, Box 176, 22100, Lund, Sweden
[d] STFC, Rutherford Appleton Laboratory, ISIS Facility, Chilton, OX11 0QX, UK

ARTICLE INFO

Keywords:
Polarized neutron imaging
Magnetic structures
Superconductivity

ABSTRACT

Polarized neutron imaging has many applications through characterization of magnetic fields generated from currents or magnetic moments. If local magnetic field directions change slowly relative to its precession frequency, the angle between neutron polarization vector and the local field vector remains constant. Conversely, if the fields change rapidly relative to the precession frequency, this angle may vary. The transition between these scenarios follows the adiabatic condition. In this study, we analyze the effects of the adiabatic condition on a polarized neutron image. Two case studies are used for illustrating possible scenarios. The first case shows how an external field, due to the adiabatic condition, influences the symmetry of a polarized neutron image of a current carrying solenoid. The second case study shows how the adiabatic coupling of the beam polarization could lead to the loss of contrast in a polarized neutron image while studying field penetration in type II superconductors. Both case studies serve to highlight the importance of taking this phenomenon into account while interpreting polarized neutron imaging data given the rising importance of the technique as a characterization method in magnetism and superconductivity research.

1. Introduction

The spin of the neutron interacts with magnetic fields making it a sensitive probe for their characterization. In addition, its charge neutrality results in a large penetration depth in many materials making the neutron an ideal tool for the characterization of magnetic fields and structures in bulk materials. Practically, the use of neutrons to this end requires the spin-polarization of a neutron beam. This involves having a majority of the neutrons in the beam with their mean spin direction aligned. The beam's polarization property is an average of the spin property of the individual neutrons in the beam. The dynamics of the beam's polarization in a static magnetic field can be shown to be analogous to that of a classical moment where the polarization precesses about an axis in the direction of the magnetic field [1]. Polarized neutron beams for imaging have mainly facilitated studies of magnetic phenomena in superconducting systems. It has been used in the visualization of the Meissner effect by Dawson et al. [2]. Beyond that, it has been instrumental in both qualitative [3] and quantitative [4] studies of field penetration and trapping in type II superconductors, both of which have proven instrumental in the materials' defect characterization [5]. In addition to superconductivity studies, it has been used in electric field characterization by Jau et al. [6] and is being explored as a means of battery characterization [7].

A polarized neutron beam traversing a spatially varying magnetic field can interact with the field either adiabatically or non-adiabatically. The nature of the interaction depends both on the magnitude of the magnetic field which determines the Larmor precession frequency of the beam polarization and the rate of change of the magnetic field direction sensed by the neutron as it traverses the field. In the case of adiabatic interaction, the polarization's Larmor precession frequency is much higher than the rate at which the magnetic field changes direction. This results in a situation where the angle between the beam polarization and the magnetic field direction is conserved through the trajectory. In experiments where the polarizer and analyzer align in the same direction, there's no detectable change in the beam's polarization. This occurs because the beam's projection onto the field direction remains consistent throughout its trajectory. Conversely, in cases where the Larmor precession frequency of the beam polarization is much lower than the rate of change of magnetic field direction, the relative orientation between the beam polarization and the changing magnetic field is not conserved in its trajectory. This means that the projection of the neutron beam polarization vector on the magnetic field vector changes. The

* Corresponding author. Institut Laue-Langevin, Large Scale Structures Group, 71 Avenue des Martyrs CS 20156, 38042, Grenoble Cedex 9, France.
E-mail address: u.oji@campus.tu-berlin.de (U.K. Oji).

https://doi.org/10.1016/j.nima.2024.169450
Received 11 March 2024; Received in revised form 27 April 2024; Accepted 13 May 2024
Available online 14 May 2024

condition for the transition from adiabatic to non-adiabatic rotation of the beam polarization can be expressed as

$$\frac{d\theta}{dt} \gg \gamma B \tag{1}$$

where $\frac{d\theta}{dt}$ is the temporal rate of change in angular direction of the magnetic field through the trajectory and γ is the gyromagnetic constant for the neutron and the product γB is the Larmor frequency of the neutron polarization, *ω,* in rad/s. The spatial rate of change, being coupled to the temporal rate of change through the neutron velocity, is determinable with knowledge of the neutron wavelength. The typical ratio between the Larmor precession and the angular rate of change terms of the equation (RHS:LHS) for the system to qualify as adiabatic is from 5 to 10 [8]. However, in proceeding discussion we simplify by considering a ratio from just above 1 to be adiabatic.

In recent years, some work has been done taking advantage of the adiabatic condition in polarized neutron imaging. Specifically, via neutron grating interferometry, a neutron Stern Gerlach experiment [9] and the measurement of strong magnetic fields taking advantage of existing field gradients [10] has been possible. There is, however, a dearth of literature that describes the effects this could have on radiography using polarized neutrons although it has had a mention in work using polarized neutrons in the visualization of compensation currents in type II superconductors [11] and electic motor characterization [12]. This paper aims to highlight, in general, potential effects the adiabatic condition can have on the results obtained from a polarized neutron imaging experiment. Two case studies are used to illustrate this. The first one involves a current carrying solenoid. We illustrate by experiment and simulation, the split between adiabatic and non-adiabatic regions for neutrons passing by the solenoid. In addition, we show how this regional split can be affected by external fields in the system and consequently modify results of the experiment. The second case study looks into the effects of the adiabatic region on the results obtained while attempting to study field penetration in a type II superconductor, specifically niobium.

2. Case 1: current carrying solenoid

The first case study for the effect of the adiabatic condition is in the investigation of the field distribution from a current carrying solenoid. The experiment was performed on the IMAT imaging station [13] of the ISIS Neutron and Muon Source. A circular neutron collimator of D = 80 mm about L ≈ 10.4 m upstream of the transmission detector results in a quasi-parallel beam with a divergence determined by an L/D of 130. The schematic in Fig. 1 illustrates the setup of the experiment comprised of a polarizer, a collimator, a spin flipper, an analyzer and the detector [14]. The polarized neutron beam size is determined by the field of view of the polarizing device (super-mirror benders) being 30 mm × 50 mm. A microchannel plate detector is used in the experiment with a pixel size of 55 µm × 55 µm with 512 × 512 pixels giving a field of view of 28 mm × 28 mm [15]. With the inclusion of the collimator, which serves also to filter the undesired spin neutrons after polarization, the effective horizontal L/D of the experiment was about 200. The polarized neutron image resolution for the experiment was about 1.2 mm. The fields from the polarizing devices are used to maintain the polarization of the neutron beam in addition to dedicated guide fields equipped with the flipper. This guide field is oriented along the z axis and is existent through the neutron trajectory, confirmed using a MagnaProbe compass. The guide field in the sample position was measured to be about 6 G using a Hall probe. The solenoid made from 1 mm diameter aluminium wire was wound by hand with a length of 12 mm, an outer diameter of 10.5 mm and 5 turns (Fig. 2 (a)). Aluminium was chosen due to its transparency to neutrons meaning it was not visible in conventional radiography which relies on absorption. The polarized neutron image obtained would therefore be dominated by the magnetic field from the conductor when current is flowing through it. With the IMAT station having a Time-Of-Flight (TOF) neutron analysis option, the mean polarization of the beam through the relevant TOF range of 30000–85000 µs, corresponding to wavelengths of 2–6 Å, is 95 %. The

solenoid is positioned at a distance 25 cm away from the detector and a current of 10 A is applied to produce a magnetic field for the polarized neutron experiment. This value of current yields a field of 42 G at the centre of the coil measured using a Hall probe. The coil axis was aligned in an orientation perpendicular to the neutron polarization and velocity.

The spin flippers facilitate acquisition of neutron radiographs for parallel and antiparallel orientations of the polarizer and analyzer during the experiment. The radiographs for the various configurations were obtained with the exposure time for each spin channel being 15 min. These facilitate the determination of the polarization image through the expression

$$P = \frac{N_{\uparrow} - N_{\downarrow}}{N_{\uparrow} + N_{\downarrow}} \tag{2}$$

Fig. 2 (b) shows polarized neutron images of the magnetic field produced by the current carrying solenoid with 10 A applied for a selection of incident neutron wavelengths. These are all normalized with the open beam polarization image. The TOF integrated polarization image is shown in Fig. 2 (c (left)). In these images, the changes in contrast indicate a resultant magnetic field from the current through the solenoid. There is also an observable pronounced asymmetry in the

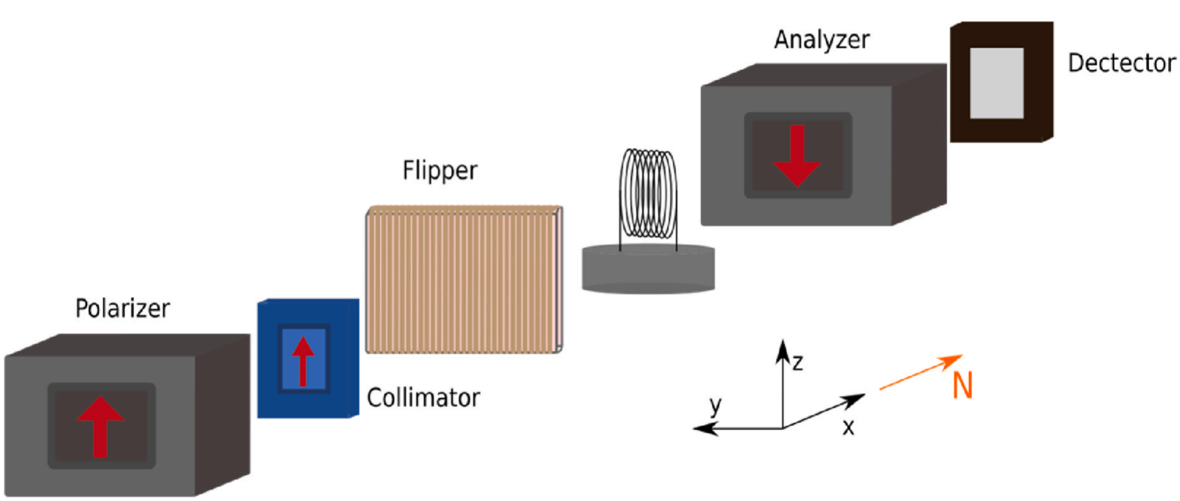

Fig. 1. Schematic of the polarized neutron imaging implementation on the IMAT beamline.

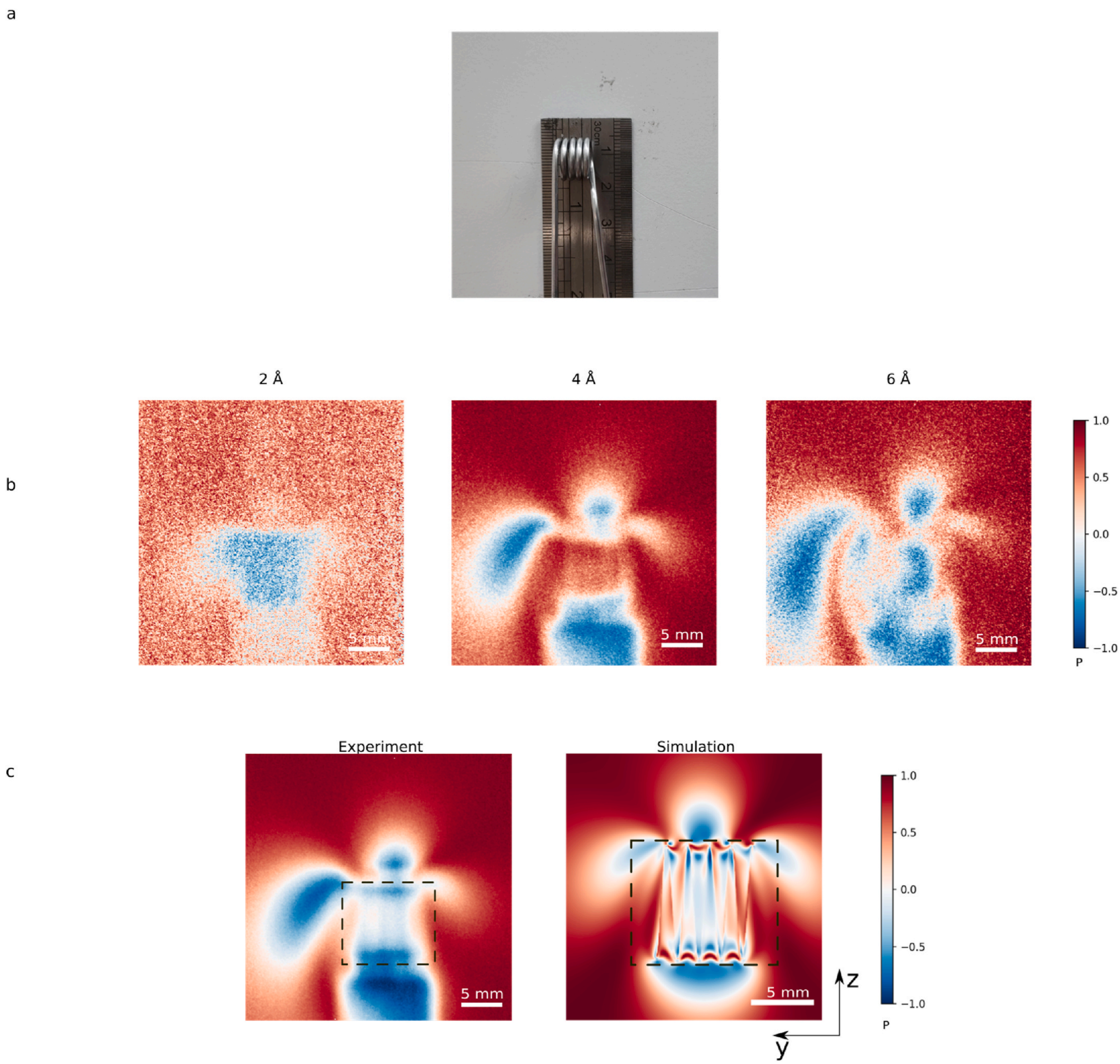

Fig. 2. (a) Aluminium coil of diameter = 10.5 mm, length = 12 mm and 5 turns (b) Polarized neutron image of the coil with I = 10 A for incident neutron wavelengths of 2 Å, 4 Å and 6 Å. (c) (left) Polarized neutron image of the coil with I = 10 A integrated through wavelengths 2–6 Å. (right) Simulated polarized neutron image integrated through wavelengths 2–6 Å of the experiment with solenoid with the same dimensions and current. There is a discrepancy in symmetry for the experimental and simulation results. The dashed boxes highlight the coil region.

polarization image in the regions of the stray field of the solenoid. This is similar to the observation by Kardjilov et al. [16] while imaging the magnetic field from a copper solenoid using a neutron beam of 4.2 Å. Further investigations for the source of the asymmetry was outside of the focal point of the work. To comprehend the origins of this asymmetry, simulations of the system are conducted and will be discussed.

The magnetic field distribution is calculated by using the Biot-Savart law that gives the magnetic field at position *r* from a current carrying element, *I*, at the origin as

$$\vec{B}(\vec{r}) = \frac{\mu_0}{4\pi}\int_C \frac{I d\vec{l} \times \vec{r}}{|\vec{r}^3|} \tag{3}$$

This gives a 3D pixel array of the magnetic vector field. With this vector field array, the TOF experiment can be simulated. The simulations were carried out using the Python programming language and involves a pixel-wise determination of the change in neutron polarization using the relation [17].

$$\vec{P}_{final} = \prod_{1}^{i=J} R\left(\vec{j_i}\right) \cdot \vec{P_0} \tag{4}$$

where *R* for each pixel, *j*, is given as

$$\begin{bmatrix} 1-(1-cos(\omega t))\cdot(1-n_x^2) & (1-cos(\omega t))n_x n_y - n_z\, sin(\omega t) & (1-cos(\omega t))n_x n_z + n_y\, sin(\omega t) \\ (1-cos(\omega t))n_x n_y + n_z\, sin(\omega t) & 1-(1-cos(\omega t))\cdot\left(1-n_y^2\right) & (1-cos(\omega t))n_y n_z - n_x (sin(\omega t)) \\ (1-cos(\omega t))n_x n_z - n_y\, sin(\omega t) & (1-cos(\omega t))n_y n_z + n_x\, sin(\omega t) & 1-(1-cos(\omega t))\cdot(1-n_z^2) \end{bmatrix} \tag{5}$$

and n_i are the unit vector components of the magnetic vector field. The simulation was performed assuming an infinitely small value of guide field to maintain the polarization level of the neutron beam through the trajectory. The initial polarization orientation was set to be in the z axis to imitate the experimental conditions.

The simulated polarization image integrated through the TOF range is shown in Fig. 2 (c (right)). Similar to the experimental results, there is a change in contrast in the image resulting from the interaction of the beam polarization with the calculated

magnetic field. On the contrary, there is no apparent asymmetry in the polarization image. This observation shows that there is more at play in the polarization image from the experiment aside the field from the solenoid with current flowing through it. A step towards understanding this observation starts with the note that a vanishingly small guide field was assumed in the simulation of the experiment. Further simulations were completed to investigate the effects adding realistic guide fields in the z direction could have on the system. Fig. 3 shows the polarization image of the system after addition of guide fields in the system up to 8 G in steps of 2 G. From these, it becomes clearer that the source of the asymmetry observed is from the guide field in the experiment.

A further question is on how the presence of the guide field contributes to the onset of an asymmetry in the system. This can be explained by evaluating the map of the adiabatic condition of the system. The field from a single x-y plane was chosen to illustrate this as is shown in Fig. 4. This choice was made because the neutron traverses along the x direction making the changes in the field direction in this direction relevant for the adiabatic condition in this experiment. The adiabatic map was simulated using the simplified form of the relation in Eq. (1) as previously described. Knowing the magnetic vector field components of the system in a pixel wise manner facilitates the determination of the angular difference in the orientation of the vector field between two pixels, θ, via

$$\theta = cos^{-1}\left(\frac{\overrightarrow{B_j}\cdot\overrightarrow{B_{j+1}}}{\left|\overrightarrow{B_j}\right|\left|\overrightarrow{B_{j+1}}\right|}\right) \tag{6}$$

Where B are the vectors of the magnetic field and j represent the pixel index values. With knowledge of the neutron velocity, the time within an element was determined, dt. This facilitates the determination of the temporal rate of change of the angular direction of the magnetic field, $\frac{d\theta}{dt}$, from pixel to pixel in the direction of the neutron beam. This can then be compared to the corresponding Larmor precession frequency of the beam polarization at the pixel to determine the regions of the simulation space where the neutron beam polarization is expected to rotate non-adiabatically from the local magnetic field. The adiabatic maps are shown in Fig. 5 for the case of the current carrying solenoid using a neutron beam of wavelength of 5.5 Å. These are binary maps where the

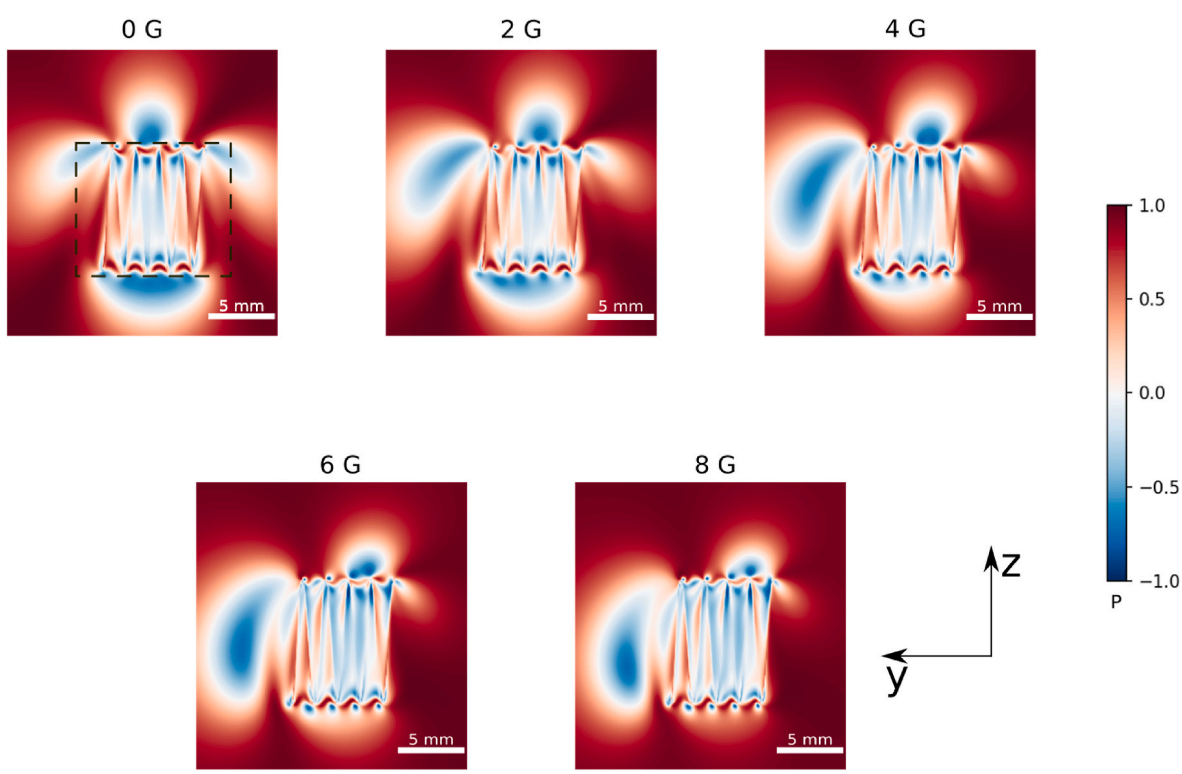

Fig. 3. Polarized neutron images integrated through wavelengths 2–6 Å with increasing values of the guide field oriented along the z axis. There is an increase in the asymmetry with increasing values of the guide field. The dashed box region highlights the solenoid.

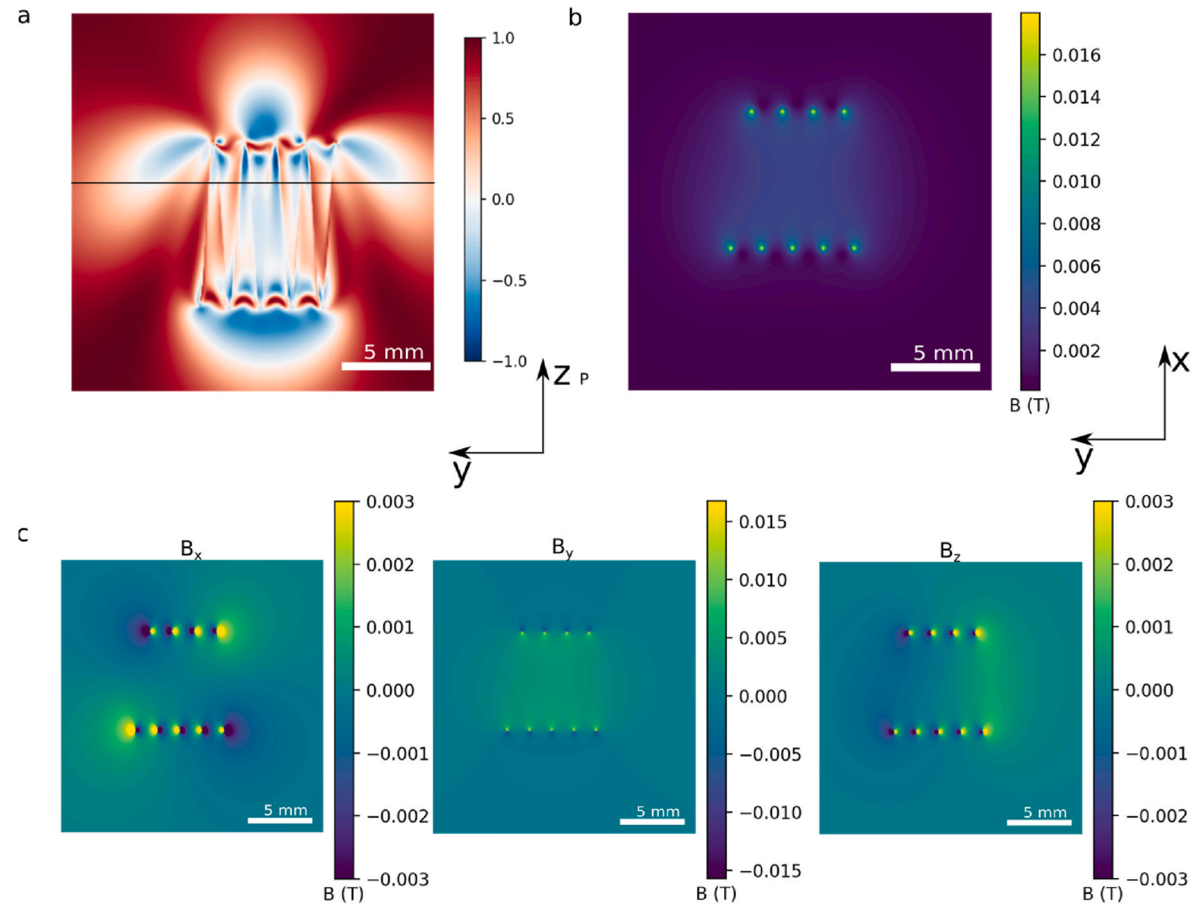

Fig. 4. (a) Simulated integrated TOF polarized neutron images of the magnetic field from the solenoid with negligible guide field. (b) Magnitude of the calculated magnetic field from current carrying solenoid of diameter = 10.5 mm, length = 12 mm and 5 turns with I = 10 A in the x-y plane as indicated by the solid black line. The adiabatic condition depends on changes in the field direction along x. (c) Magnetic vector field components of (b). B_x and B_z colourbar saturation adjusted to highlight sign changes.

pixels with values 0 and 1 represent those where the angle between magnetic and polarization vectors are conserved (adiabatic coupling) and not conserved (non-adiabatic rotation) respectively.

Looking at the map of the adiabatic condition, it is observed that, even in the case of an infinitely small guide field (0 G), there is an existing asymmetry in the system which could be a result of the coil having 4 turns at the top and 5 at the bottom (Fig, 2 (a)). This asymmetry becomes more pronounced on increasing the value of the guide field as can be observed in the image. This effect is a direct consequence of the adiabatic condition and is consistent across the relevant wavelength range. This consistency is illustrated in Fig. 6 where the adiabatic map for different neutron wavelengths is shown for the system in a guide field of 4 G. It is observed that with a guide field present, there is a significant asymmetry in the system with higher values of neutron wavelength. This happens because at higher wavelengths, the neutron beam has a lower velocity resulting in a reduced angular change in direction experienced by the neutron as it interacts with the magnetic field. Consequently, the Larmor precession becomes more significant in determining the adiabatic map. From Fig. 4 (c), we see that the inclusion of the guide field in the z direction would lead to the increased asymmetry in the B_z component of the magnetic vector field accounting for the observation.

3. Case 2: superconducting wire

The importance of considering the adiabatic condition in polarized neutron imaging was further underscored via an investigation of flux penetration in a 1 mm radius superconducting niobium wire with no current flowing through it.

The experiment was carried out on the D33 small angle neutron scattering (SANS) instrument at the Institut Laue Langevin. The sample-detector distances allowed its use in projection imaging of materials due to the magnification capability. The 256 × 128 pixel detector was used where the pixels have dimensions of 2.5 mm × 5 mm. The basic polarization setup was similar to that on the IMAT station, with the inclusion of a cryomagnet at the sample position. The incident polarized neutrons had a wavelength of 5.5 Å and were analyzed after interaction with a magnetic field by a ^{3}He polarization analyzer [18,19] and before recording of a projection image in the detector. Inversion of the incident neutron beam polarization direction was facilitated by the use of flippers installed before the sample. The flipping ratio of the setup, defined as the ratio of open beam transmissions for parallel and antiparallel orientations of initial and final polarization states, was found to be 11. This value indicates that the polarized beam was adequate for the polarized neutron imaging experiment. The sample position was located at a distance of 13.6 m from the detector. The cryomagnet at the sample position enabled both cooling of the superconductor to a temperature of 4 K and provision of a magnetic field. Illustrated in Fig. 7 (a), the incident neutron beam polarization is oriented in the same direction as the neutron velocity and applied field, all of which are perpendicular to the wire axis. Further, Fig. 7 (b) shows a calculated magnetic field distribution of a superconducting wire with the same dimensions in a magnetic field of about 200 G to illustrate the Meissner effect. In addition, the adiabatic map is shown for an incident neutron wavelength of 5.5 Å. The model used is based on the work by Fiolhas and Essen [20] wherein, in polar coordinates, the magnetic vector field distribution is given by

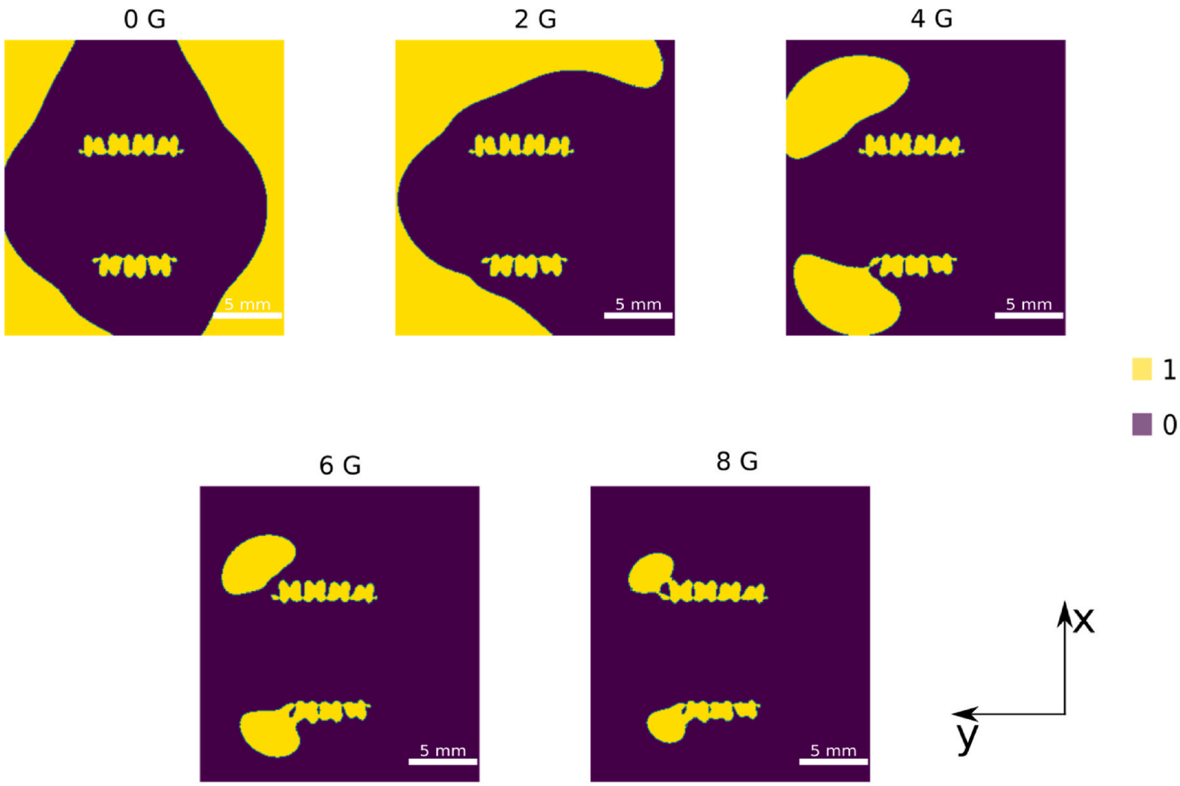

Fig. 5. Adiabatic condition maps as a function of increasing guide fields of the slice of the x-y plane as indicated by the solid black line using a neutron beam with λ = 5.5 Å.Observable effect of the guide field on the split between regions of adiabatic coupling (0) and non-adiabatic rotation (1).

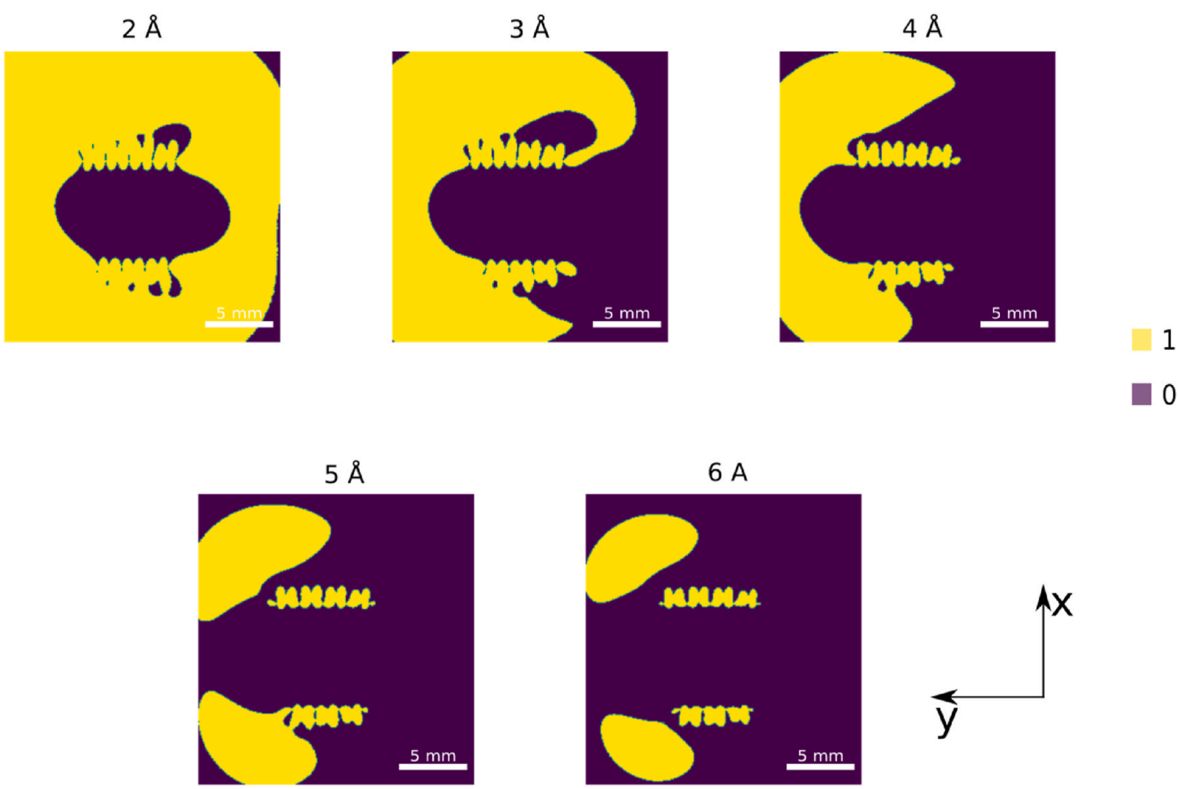

Fig. 6. Simulation of the adiabatic map dependency on the neutron beam wavelength with a guide field of 4 G applied. The effect of the guide field on the system symmetry is consistent through the relevant wavelengths.

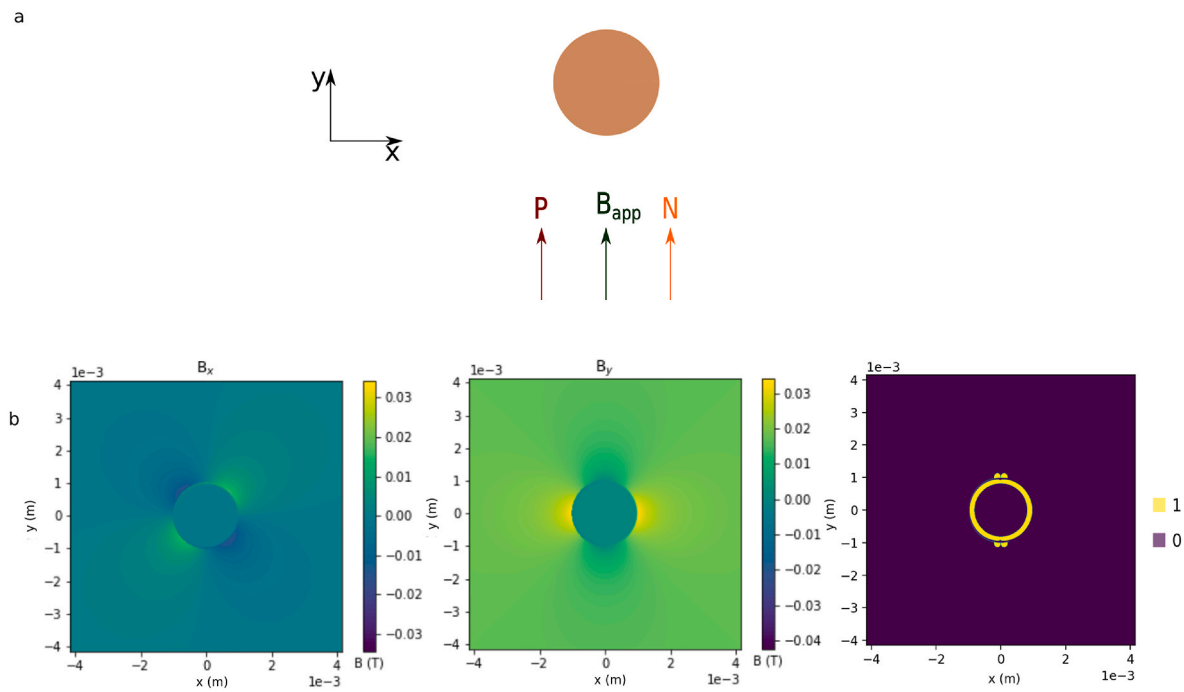

Fig. 7. (a) Schematic illustration of the experimental geometry illustrating the relative orientations of the superconducting wire, the direction of the applied field, the neutron beam polarization and the neutron velocity direction. (b) Simulation of the magnetic field distributions from the experimental geometry for an applied field of 200 G showing the magnitudes of the non-zero components of the vector field. The map of the regions of adiabatic (0) and non-adiabatic rotation (1) in addition to an illustration of the magnetic field vector field are included.

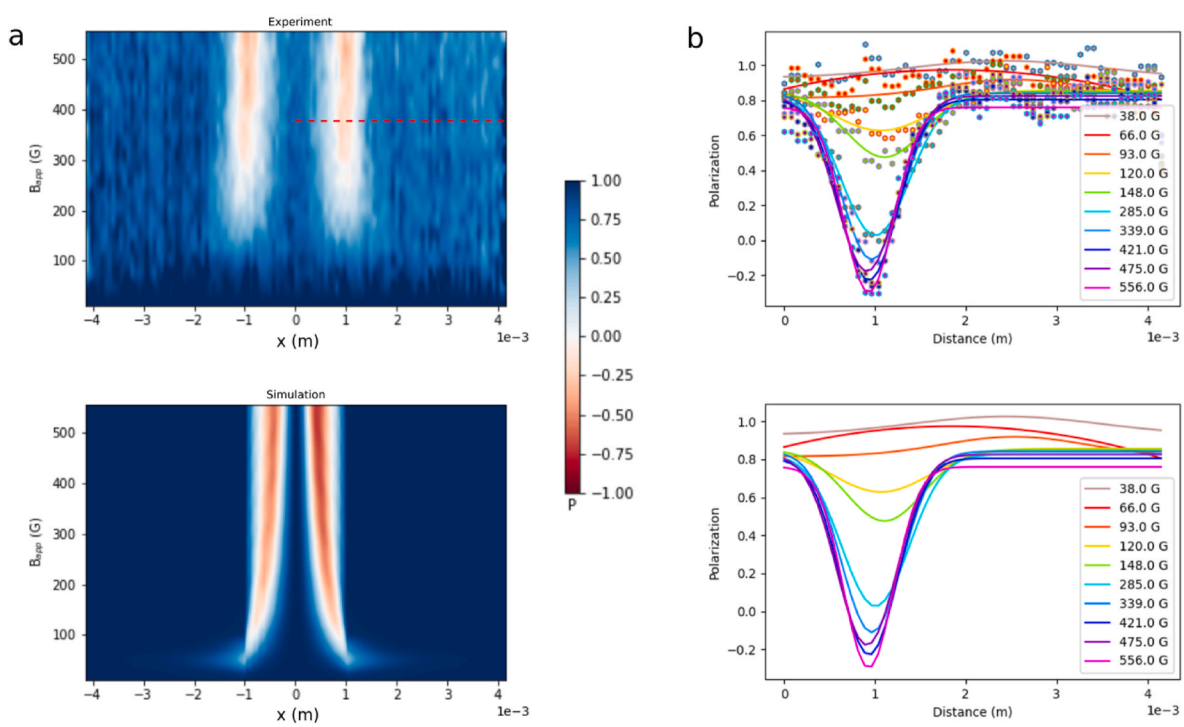

Fig. 8. (a) Mean (along the z axis) final polarization at the detector as a function of the applied field (top) and the corresponding simulations of the same quantity (bottom). (b) Graphs of the mean polarization as a function of the applied magnetic field including Gaussian fits of the profiles (top), and solely Gaussian fits of the polarization profiles for clarity (bottom). The non-adiabatic rotation of the neutron beam starts at a field of about 120 G and there is a steady shift of the peak with increasing magnitude of the applied field.

$$\overrightarrow{B}_{\rho>R} = B_0\left(1-\frac{R^2}{\rho^2}+2\lambda\frac{R}{\rho^2}\frac{I_1(R/\lambda)}{I_0(R/\lambda)}\right)sin\,\varphi\hat{\rho} + B_0\left(1+\frac{R^2}{\rho^2} - 2\lambda\frac{R}{\rho^2}\frac{I_1(R/\lambda)}{I_0(R/\lambda)}\right)cos\,\varphi\hat{\varphi} \quad (7)$$

$$\overrightarrow{B}_{\rho<R} = 2B_0\left(\frac{\lambda}{\rho}\frac{I_1(\rho/\lambda)}{I_0(R/\lambda)}\right)sin\,\varphi\hat{\rho} + 2B_0\left(\frac{I_0(\rho/\lambda)}{I_0(R/\lambda)} - \frac{\lambda I_1(\rho/\lambda)}{\rho I_0(R/\rho)}\right)cos\,\varphi\hat{\varphi} \quad (8)$$

where φ represents the polar angle, ρ represents the radial distance and $\hat{\varphi}$ and $\hat{\rho}$ are the unit vectors in the polar and radial directions, respectively. R is the radius of the superconducting wire, λ is the penetration depth, B_0 is the field applied in the system and I_n are the modified Bessel functions. A particular limitation with this model is that it adopts a higher value of penetration depth than is physically accurate. This is however not an obstacle for its use in a qualitative study of the system in question. In fact, on conversion to Cartesian coordinates, the distribution of the x component of the magnetic field distribution is visually similar to the results obtained from the polarized neutron image of the Meissner effect by Dawson et al. [2]

For the experiment, the field from the cryomagnet was increased from 16 G, its remnant value, to 560 G. The polarized neutron images obtained are normalized with open beam polarization images. Furthermore, in principle, there is no dependence of the field on the z axis so it is instructive to plot the profiles of the polarized neutron

image averaged along this axis (this also improves the statistics). The pixel resolution along the x axis is about 73 μm. The evolution of these profiles with applied field is shown in Fig. 8 (a). The effect of the adiabatic condition is first observed at lower field values which appear to result in no change in contrast of the polarized neutron image. Though it may appear so, the Meissner effect is not suppressed at the lower values of applied magnetic field [21]. Based on the adiabatic map (Fig. 7 (b)), the beam polarization should be coupled to the magnetic field everywhere in the system with the exception of the wire edges. For the low field values, it is likely that the levels of field inhomogeneity are not sufficient for the condition for non-adiabatic rotation to be fulfilled, similar to what has been observed by Jacobo et al. [11]. This changes when the field is increased to a value of 120 G for which there is a

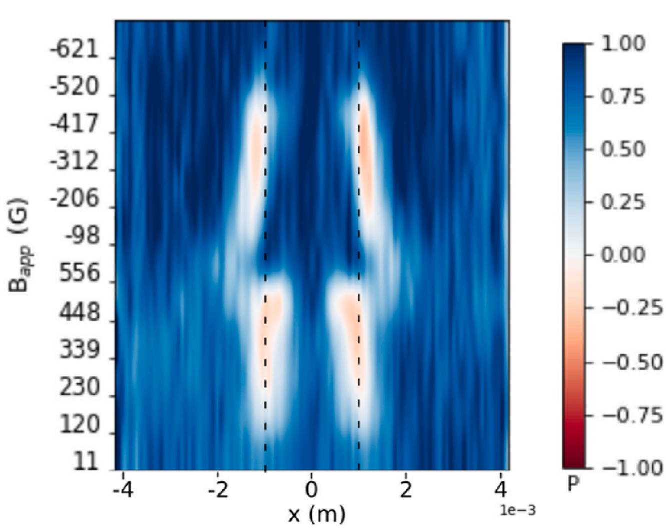

Fig. 9. Evolution of the mean polarization profiles at the detector as a function of the applied magnetic field showing the initial increase of the magnetic field and then the subsequent application of field in the reverse direction. Reversal of the applied magnetic field results in the expulsion of the magnetic field in the wire and the subsequent increase of the reversed field restarts the penetration process. At sufficiently high magnitudes (~500 G), the field penetrates the wire. This manifests itself as a loss of the signal indicating an adiabatic coupling of the neutron beam polarization with the magnetic field from an increase in homogeneity in the field distribution.

change in polarization of the neutron beam at the edges of the wire. This is also observed in simulations (Fig. 8(a)) for lower field values.

With the applied magnetic field surpassing the expected penetration field (≈400 G) with no apparent change in contrast in the polarized neutron image, a

reversed field was applied to the system with the full evolution of the polarized neutron image including the field reversal shown in Fig. 9. From the image shown in Fig. 8 (a), there is no apparent field penetration for all values of field applied and the Meissner effect is the only observable, however, the result shown in Fig. 9 suggests something to the contrary. This being that the field starts to penetrate the wire. This observation is corroborated by the indication of an expulsion of the magnetic field on reversal of the direction of applied magnetic field. In addition, a look at the polarization profiles along the x axis indicated by the red dashed line for selected values of applied magnetic field prior to field reversal (Fig. 8 (b)) shows a progressive shift in the peaks towards the centre of the wire as the field value is increased from about 420 G (before the field direction reversal). This is indicative of a flux penetration in the wire.

Again, the effect of the adiabatic condition is observed on increasing the value of the reversed magnetic field. At a field value of about −520 G, the image contrast appears to disappear completely. This, like the non-detection of the Meissner effect earlier can be ascribed to effects from the adiabatic coupling of the neutron beam polarization to the field on the polarized neutron image. When the field starts to penetrate into the wire, the level of inhomogeneity in direction of the magnetic field, which was initially high at the wire edges due to the Meisnner effect, is then reduced ultimately resulting in the adiabatic coupling of the beam polarization to the magnetic field, with no apparent change in the beam polarization at the detector beyond −520 G.

4. Conclusion

We have demonstrated the effects of the adiabatic condition in polarized neutron imaging. Following a discussion of the mechanisms involved, two case studies were used to showcase different sides of the condition and to highlight potential limitations it can impose on polarized neutron imaging. The case of the normal conducting wire shows how an asymmetry can develop due to changes in regions of non-adiabatic rotation and the case of the superconducting wire demonstrates how the signal can be lost due to homogenization of the field to be characterized. However, the effect can be used practically. In characterization of materials where the objective is the study of internal magnetization, adiabatic coupling can be taken advantage of to limit the effects of the stray field from the material on the resultant polarized neutron image.

CRediT authorship contribution statement

U.K. Oji: Writing – review & editing, Writing – original draft, Visualization, Methodology, Investigation, Formal analysis, Conceptualization. **A. Backs:** Investigation. **W. Kockelmann:** Writing – review & editing, Resources, Investigation. **I. Manke:** Supervision, Resources. **A. Hilger:** Software, Resources, Formal analysis. **N. Kardjilov:** Writing – review & editing, Supervision, Investigation. **R. Cubitt:** Writing – review & editing, Supervision, Investigation, Conceptualization.

Declaration of competing interest

The authors declare that they have no known competing financial interests or personal relationships that could have appeared to influence the work reported in this paper.

Data availability

Data will be made available on request.

Acknowledgements

We are grateful for the support by G.J. Nilsen, K. Nemkovski, M. Devonport (ISIS Polarization Group), D.E. Pooley (ISIS Detector Group), J. Lewis (ISIS Mechanical Support Group) and J. Nutter (ISIS Electrical Support and Motion Control). The STFC Rutherford Appleton Laboratory is thanked for access to neutron beam facilities (IMAT/RB2210226, DOI 10.5286/ISIS.E.RB2210226). In addition, we acknowledge the support of M. Bonnaud (ILL) for experimental support. Instrumentation develop-ment for this project was jointly funded by the Institut Laue Langevin, the Helmholtz Zentrum Berlin and ISIS Neutron and Muon Source.

References

[1] J.T. Cremer, Introduction, in: Neutron and X-Ray Optics, Elsevier, 2013, pp. 1–160, https://doi.org/10.1016/B978-0-12-407164-3.00019-X.

[2] M. Dawson, I. Manke, N. Kardjilov, A. Hilger, M. Strobl, J. Banhart, Imaging with polarized neutrons, New J. Phys. 11 (4) (2009) 043013, https://doi.org/10.1088/1367-2630/11/4/043013.

[3] N. Kardjilov, I. Manke, M. Strobl, A. Hilger, W. Treimer, M. Meissner, T. Krist, J. Banhart, Three-dimensional imaging of magnetic fields with polarized neutrons, Nat. Phys. 4 (5) (2008) 399–403, https://doi.org/10.1038/nphys912.

[4] A. Hilger, I. Manke, N. Kardjilov, M. Osenberg, H. Markötter, J. Banhart, Tensorial neutron tomography of three-dimensional magnetic vector fields in bulk materials, Nat. Commun. 9 (1) (2018) 4023, https://doi.org/10.1038/s41467-018-06593-4.

[5] A.E. Ţuţueanu, M. Sales, K. Eliasen, M.E. Lăcătuşu, J.-C. Grivel, N. Kardjilov, I. Manke, M. Krzyzagorski, Y. Sassa, M. Andersson, S. Schmidt, K. Lefmann, Non-destructive characterisation of dopant spatial distribution in cuprate superconductors, Physica C 575 (2020) 1353691, https://doi.org/10.1016/j.physc.2020.1353691.

[6] Y.-Y. Jau, D.S. Hussey, T.R. Gentile, W. Chen, Electric field imaging using polarized neutrons, Phys. Rev. Lett. 125 (11) (2020) 110801, https://doi.org/10.1103/PhysRevLett.125.110801.

[7] R.F. Ziesche, N. Kardjilov, W. Kockelmann, D.J. Brett, P.R. Shearing, Neutron imaging of lithium batteries, Joule 6 (1) (2022) 35–52, https://doi.org/10.1016/j.joule.2021.12.007.

[8] S. Grigoriev, A. Okorokov, V. Runov, Peculiarities of the construction and application of a broadband adiabatic flipper of cold neutrons, Nucl. Instrum. Methods Phys. Res. Sect. A Accel. Spectrom. Detect. Assoc. Equip. 384 (2–3) (1997) 451–456, https://doi.org/10.1016/S0168-9002(96)00919-9.

[9] J. Valsecchi, M.G. Makowska, Y. Kim, S.W. Lee, C. Grünzweig, F.M. Piegsa, M. A. Thijs, J. Plomp, M. Strobl, Decomposing magnetic dark-field contrast in spin analyzed Talbot-Lau interferometry: a Stern-Gerlach experiment without spatial beam splitting, Phys. Rev. Lett. 126 (7) (2021) 070401, https://doi.org/10.1103/PhysRevLett.126.070401.

[10] J. Valsecchi, R.P. Harti, M. Raventós, M.D. Siegwart, M. Morgano, P. Boillat, M. Strobl, P. Hautle, L. Holitzner, U. Filges, W. Treimer, F.M. Piegsa, C. Grünzweig, Visualization and quantification of inhomogeneous and anisotropic magnetic fields by polarized neutron grating interferometry, Nat. Commun. 10 (1) (2019) 3788, https://doi.org/10.1038/s41467-019-11590-2.

[11] J. Valsecchi, J.S. White, M. Bartkowiak, W. Treimer, Y. Kim, S.W. Lee, D. M. Gokhfeld, R.P. Harti, M. Morgano, M. Strobl, C. Grünzweig, Visualization of compensating currents in type-II/1 superconductor via high field cooling, Appl. Phys. Lett. 116 (19) (2020) 192602, https://doi.org/10.1063/5.0004438.

[12] K. Hiroi, T. Shinohara, H. Hayashida, J.D. Parker, K. Oikawa, M. Harada, Y. Su, T. Kai, Magnetic field imaging of a model electric motor using polarized pulsedneutrons at J-PARC/MLF, Journal of Physics: Conference Series 862 (2017), https://doi.org/10.1088/1742-6596/862/1/012008, 012008.

[13] W. Kockelmann, T. Minniti, D. Pooley, G. Burca, R. Ramadhan, F. Akeroyd, G. Howells, C. Moreton-Smith, D. Keymer, J. Kelleher, S. Kabra, T. Lee, R. Ziesche, A. Reid, G. Vitucci, G. Gorini, D. Micieli, R. Agostino, V. Formoso, F. Aliotta, R. Ponterio, S. Trusso, G. Salvato, C. Vasi, F. Grazzi, K. Watanabe, J. Lee, A. Tremsin, J. McPhate, D. Nixon, N. Draper, W. Halcrow, J. Nightingale, Time-of-Flight neutron imaging on IMAT@ISIS: a new user facility for materials science, J. Imag. 4 (3) (2018) 47, https://doi.org/10.3390/jimaging4030047.

[14] U. Oji, V. Pacheco, M. Sahlberg, A. Backs, R. Woracek, D. Pooley, G. Nilsen, K. Nemkovski, W. Kockelmann, A. Tremsin, A. Hilger, R. Ziesche, I. Manke, R. Cubitt, N. Kardjilov, Implementation of time of flight polarized neutron imaging at IMAT-ISIS, Mater. Des. (2023) 112429, https://doi.org/10.1016/j.matdes.2023.112429.

[15] A.S. Tremsin, J.V. Vallerga, J.B. McPhate, O.H.W. Siegmund, R. Raffanti, High resolution photon counting with MCP-timepix quad parallel readout operating at > 1 KHz frame rates, IEEE Trans. Nucl. Sci. 60 (2) (2013) 578–585, https://doi.org/10.1109/TNS.2012.2223714.

[16] N. Kardjilov, A. Hilger, I. Manke, M. Strobl, M. Dawson, J. Banhart, New trends in neutron imaging, Nucl. Instrum. Methods Phys. Res. Sect. A Accel. Spectrom. Detect. Assoc. Equip. 605 (1- 2) (2009) 13–15, 10.1016/j.nima.2009.01.162.

[17] M. Th Rekveldt, Study of ferromagnetic bulk domains by neutron depolarization in three dimensions, Z. Phys. 259 (5) (1973) 391–410, 10. 1007/BF01397376.

[18] W. Heil, K. Andersen, D. Hofmann, H. Humblot, J. Kulda, E. Lelievre-Berna, O. Schärpf, F. Tasset, 3He neutron spin filter at ILL, Phys. B Condens. Matter 241–243 (1997) 56–63, https://doi.org/10.1016/S0921-4526(97)00511-5.

[19] F. Tasset, Towards helium-3 neutron polarizers, Phys. B Condens. Matter 213–214 (1995) 935–938, https://doi.org/10.1016/0921-4526(95)00327-6.

[20] M.C. Fiolhais, H. Essén, Magnetic field expulsion from an infinite cylindrical superconductor, Physica C (Amsterdam, Neth.) 497 (2014) 54–57, https://doi.org/10.1016/j.physc.2013.11.006.

[21] S. Aull, O. Ebrahimi, N. Karakas, J. Knobloch, O. Kugeler, W. Treimer, Suppressed Meissner-effect in niobium: visualized with polarized neutron radiography, J. Phys. Conf. 340 (2012) 012001, https://doi.org/10.1088/1742-6596/340/1/012001.